Available online at www.sciencedirect.com
ScienceDirect
Polymer 47 (2006) 7477–7484
polymer
www.elsevier.com/locate/polymer

A study of global vs. local properties for maleic anhydride modified polypropylene nanocomposites

Shing-Chung Wong [a,*], Hyukjae Lee [b], Shiyue Qu [a], Shankar Mall [c], Ling Chen [d]

[a] Department of Mechanical Engineering, University of Akron, Akron, OH 44325-3903, USA
[b] School of Advanced Materials Engineering, Andong National University, Gyungbuk, South Korea
[c] Department of Aeronautics and Astronautics, Air Force Institute of Technology, 2950 P. St, Building 640, Wright Patterson AFB, OH 45433, USA
[d] Institute of Materials Research and Engineering, 3 Research Link, Singapore 117602, Singapore

Received 21 May 2006; received in revised form 21 August 2006; accepted 21 August 2006
Available online 8 September 2006

Abstract

Nanoindentation of organomodified clay filled maleated polypropylene (MAPP) was investigated. The study aims to identify the relative increase in local stiffness in comparison to the increase in mechanical properties of the bulk in polypropylene-based nanocomposites. Such a study allows one to assess confined material property in addition to increased filler volume at the local scale. A mixture of highly intercalated and well exfoliated clay structures, when dispersed in MAPP matrix, was observed under transmission electron microscopy. The degree of exfoliation was found to increase with clay loading, which was attributed to the higher viscosity and mechanical shear forces during melt compounding. Instrumented indentation was performed on (1) clay aggregate supported by MAPP matrix, (2) clay–matrix boundary, and (3) the MAPP matrix. The clay aggregated region generally showed higher stiffness as compared to the matrix. And, the relative increase in indentation stiffness is substantially higher than the relative increase in tensile and compressive stiffnesses for clay reinforced systems. Polymer chain confinement and topological constraint appeared to be operative to enhance local stiffness in the clay aggregated region. Good correlation was, however, obtained between the change in macroscopic stiffness and the change in highly local indentation stiffness as a result of clay reinforcement.

Keywords: Polymer nanocomposites; Polypropylene; Nanoindentation

1. Introduction

Recent advances in polymers reinforced by organomodified clays have shown that the polymer nanocomposites derived thereof possess attractive attributes such as enhanced mechanical strength and stiffness [1–3], improved fracture toughness performance [4–6], and barrier performance [7–9]. Little is understood on the local mechanical performance vs. global deformation of polymer nanocomposites [10]. Global deformation is defined herein as the macroscopic elastic stiffness, which is quantified by the Young's modulus, at the beginning of deformation. And, in this paper, we present results from both tensile and compressive modes of loading in comparison to local indentation loading. A notion has been suggested that inference of mechanical properties such as dynamic mechanical properties can be made directly from local indentations of polymers [11] or the notion can be modified by a scaling law in polymeric materials. If true, this would allow assessment of mechanical properties using miniaturized specimens. However, it has been noted that local composite properties in a confined region may introduce strengthening mechanisms not predicted by composite theory, which mainly takes into account filler volume fractions and not matrix stiffening effect due to molecular chain confinement and/or topological constraint. In this study, we compare global and local stiffening behaviors and evaluate if indeed local property is influenced by filler volume fraction alone or not.

* Corresponding author. Tel.: +1 330 972 8275; fax: +1 330 972 6027.
E-mail address: swong@uakron.edu (S.-C. Wong).

0032-3861/$ - see front matter © 2006 Elsevier Ltd. All rights reserved.
doi:10.1016/j.polymer.2006.08.049

Success for processing polymer nanocomposites is most notably demonstrated in nylon 6 [2,3] and, more recently, in smectite clay reinforced epoxy [12,13]. Polypropylene is one of the most cost-effective commodity plastics and it is in high demand in the world market. However, the non-polar nature of polypropylene creates challenges for uniformly and disorderly exfoliated nanoclay platelets to be formed [14,15]. This study demonstrates mixtures of intercalated and exfoliated nanoclay structures dispersed in maleic anhydride modified polypropylene. From the relationship between local indentation stiffness and global tensile and compressive properties, we could gain some insight into the influence of clays on local vs. global deformations for polymer nanocomposites, the understanding of which can be fruitful for polymer testing and future applications in scratch resistant polymers and polymer–clay interactions. Electron microscopy is employed to directly examine the clay dispersion and exfoliation in maleated PP. An instrumented indenter that can perform continuous stiffness measurement (CSM) is used to indent on the selected areas of interest. Local and global elastic moduli are compared.

2. Experimental work

2.1. Materials

The matrix materials studied were commercially available maleic anhydride modified polypropylene (MAPP) (polybond 3200) from Crompton. The organoclay (Nanomer I.31PS onium ion modified montmorillonite clay), which was modified with octadecylamine, was supplied from Nanocor Inc. MAPP was chosen over unmaleated PP for its acid content and reactivity, enhancing the interfacial bonding between PP and organomodified montmorillonite. Our previous studies on mechanical and fracture properties were also performed on MAPP and the current study forms part of a series of research efforts conducted in USA and Singapore [1,4,14]. The physical properties of the as-received MAPP used in this study are given in Table 1.

Maleic anhydride modified polypropylene and organoclay were melt compounded in a counter-rotating intermeshing twin screw extruder (Leistritz LSM 34GG, $L/D = 32.5$). The compounding temperature was 180 °C to produce the masterbatch containing 10 wt% clay, followed by recompounding with fresh maleated PP to obtain MAPP nanocomposites at 0, 2.5, 5, 7.5 and 10 wt% clay loadings. The blended samples were re-extruded to achieve more uniform dispersion. Materials were injection molded into 3.5-mm thick dumbbell specimens (Type V specimens according to ASTM standard D638-02a) and 3.00-mm thick rectangular specimens. All materials were dried at 80 °C in a vacuum oven for at least 16 h, prior to compounding and injection molding.

Table 1
Physical properties of maleated polypropylene (MAPP)

Grade/supplier	Polybond® 3200/Crompton
Melt flow rate (g/min)	11
Melting temp. (°C)	157
Density at 23 °C (g/ml)	0.91

2.2. Transmission electron microscopy

To examine the morphology of the nanocomposites, ultrathin sections with thicknesses of 80–100 nm were cut from the molded samples using a Leica Ultracut UCT microtome. Then the sections were picked up with 200 mesh formvar/carbon coated copper grids and observed under a Philips CM 300 TEM at an accelerating voltage of 300 kV. Image analysis was used to assess the increase in filler content in the clay–polymer intercalated region based on the TEM micrographs. The area fraction was obtained using the software ImageJ (Image Processing and Analysis in Java). The area of interest was converted into a binary (black and white) image which assumes that clay platelets are black and background is white. The software scans the image until it finds the edge of an object. The area fraction was automatically calculated from the measurement.

2.3. Mechanical tests

To compare local vs. global deformation, tensile and compressive tests of bulk specimens were performed according to ASTM standards using an Instron Model 5567 computer-controlled testing machine equipped with an extensometer. The crosshead speed was kept constant at 0.08 mm/min at ambient temperature. At least five specimens of each composition were tested. Compression tests were also conducted in this study at the same crosshead speed.

2.4. Nanoindentation

Nanoindentation tests were conducted on MTS Nanoindenter XP using a Berkovich indenter tip on polished nanocomposite samples. The nanoindenter has displacement and load resolutions of 0.01 nm and 50 nN, respectively. Dynamic Contact Module (DCM) option offers high precision and resolution such that the displacement and load resolutions of DCM are 0.0002 nm and 1 nN, respectively. A total of 15 indentations were conducted on each specimen using the continuous stiffness measurement (CSM) technique [16] and the average values of 15 indentations are presented in the present study. In some specimens, indentations with DCM option were also employed to verify the results from XP module. The CSM allows the measurement of dynamic stiffness continuously throughout the loading segment by superimposing a small dynamic oscillating displacement on top of the quasi-static force by means of a frequency-specific amplifier. This technique measures the contact stiffness at any point of the quasi-static loading curve and not just at the point of unloading as in other models of nanoindentation. The area function (A) of the Berkovich tip, which depends on indenter shape and is also known as the indenter shape function, is represented by:

$$A(h) = C_0h^2 + C_1h + C_2h^{1/2} + C_3h^{1/4} + \cdots + C_8h^{1/128} \quad (1)$$

where $C_0 \ldots C_8$ are constants determined by curve fitting, and h is the indentation depth. $A(h)$ allows for the calculations of the elastic modulus, which is reported in the current study, and hardness [16]. Note that the contact area is automatically calculated by the indenter software for each indentation experiment.

An indentation test is composed of several segments. In the first segment the indenter tip approached the surface of the specimen while the surface was located by the change in stiffness. In the next segment, the indentation load was applied with a constant strain rate of 0.05/s up to a depth of 4000 nm with a harmonic displacement of 2 nm at 45 Hz. After a 10 s hold at the maximum load, the unloading segment proceeded until 90% of the maximum load was removed, after which another 10 s hold was applied for the thermal drift correction. The indentation test was then completed after 100% unloading. When DCM option was employed, the oscillation displacement, the frequency and the maximum indentation depth were 1 nm, 75 Hz, and 700 nm, respectively.

3. Results and discussion

This study examines directly the local morphology of nanoclay reinforced MAPP and their subsequent local mechanical properties. The mechanical properties and fracture toughness of the bulk of a similarly prepared MAPP-based system were reported earlier [1,4] but the MAPP used previously was different from the current study as specified in Section 2.1. The maleic anhydride modified PP aims to enhance interaction between the hydrophilic clays and hydrophobic PP. To aid our discussion on instrumented indentation properties, the clay morphology is revealed using TEM herein so that one can gain understanding of where and how instrumented indentations were performed. Fig. 1 compares the low magnification TEM micrograph and high magnification TEM micrograph of 2.5 wt% reinforced MAPP. The intercalated and exfoliated morphology of nanoclay reinforced MAPP is evidently illustrated. Clay aggregates (Fig. 1a), when enlarged (Fig. 1b), show clearly the highly intercalated morphology, which is consistent with the clay morphology of other PP-based systems [14,15]. Some sparsely exfoliated clay structures can also be observed. In our study, the exfoliation is not optimized until a higher loading of clay is introduced. Figs. 2–4 show the clay morphology at 5, 7.5 and 10 wt% reinforcements, respectively. From the TEM micrographs, it appears that the clay platelets become more uniformly dispersed as clay loading increases, see Figs. 3 and 4. And extensive exfoliation of maleated PP nanocomposite is evident at 7.5 and 10 wt% loadings of clays, see Figs. 3b and 4b. This is attributed to the higher viscosity, which in turn produces higher mechanical shear forces, as clay loading increases in the extrusion process. The mechanical shear forces appear essential for good exfoliation of clays in polypropylene-based system, as the driving force from chemical interactions is insufficient to expand and exfoliate the clays completely.

The observed morphology as a function of the clay loading also casts light in our previously reported fracture toughness

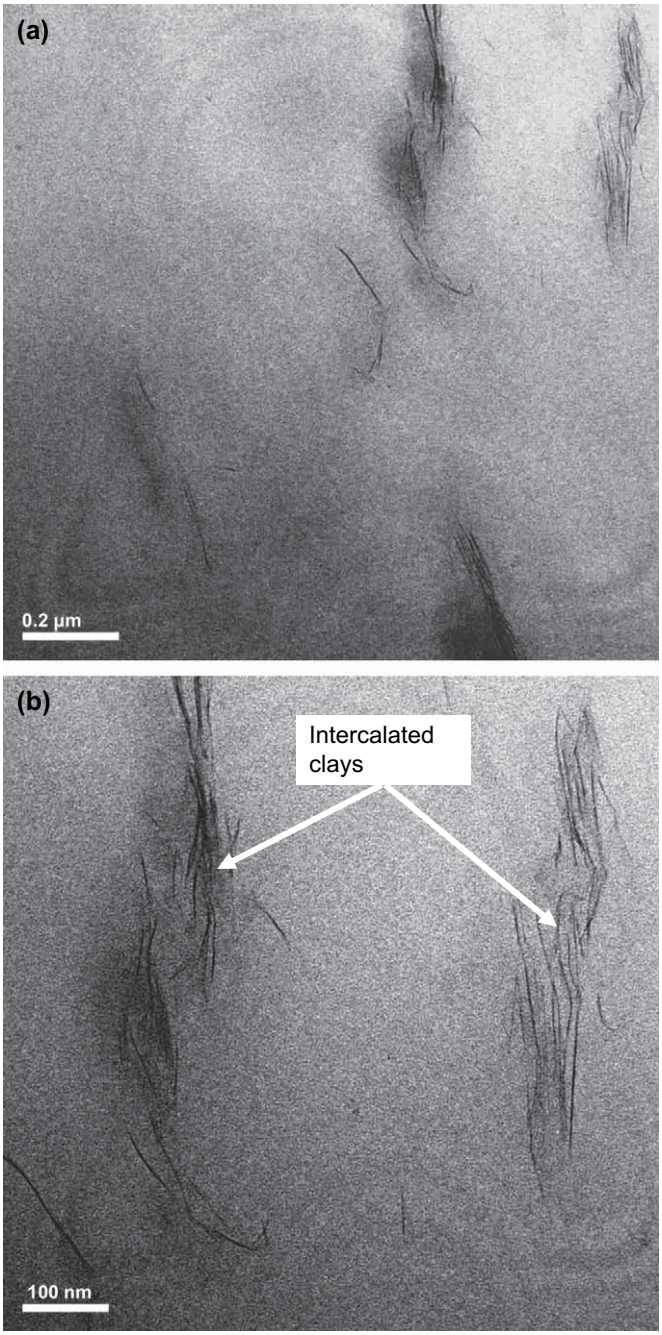

Fig. 1. TEM photomicrographs of 2.5 wt% clay reinforced maleated PP: (a) low magnification and (b) high magnification. The micrographs demonstrate a mixture of clay aggregated intercalation and sparsely exfoliated clay structures in MAPP.

[1,4]. Our previous work showed that the fracture toughness, represented by the non-linear elastic J-integral fracture toughness, and molecular deformation as evident in small-angle X-ray scattering (SAXS) were enhanced in the presence of 2.5 wt% clay loading. Thereafter, the toughness drops considerably and molecular deformation becomes increasingly constrained as clay loading increases. The small clay loading, say 2.5 wt%, is unique in enhancing the toughness of increasingly exfoliated nanocomposite system. Such a small clay loading is consistent with the fracture toughness results

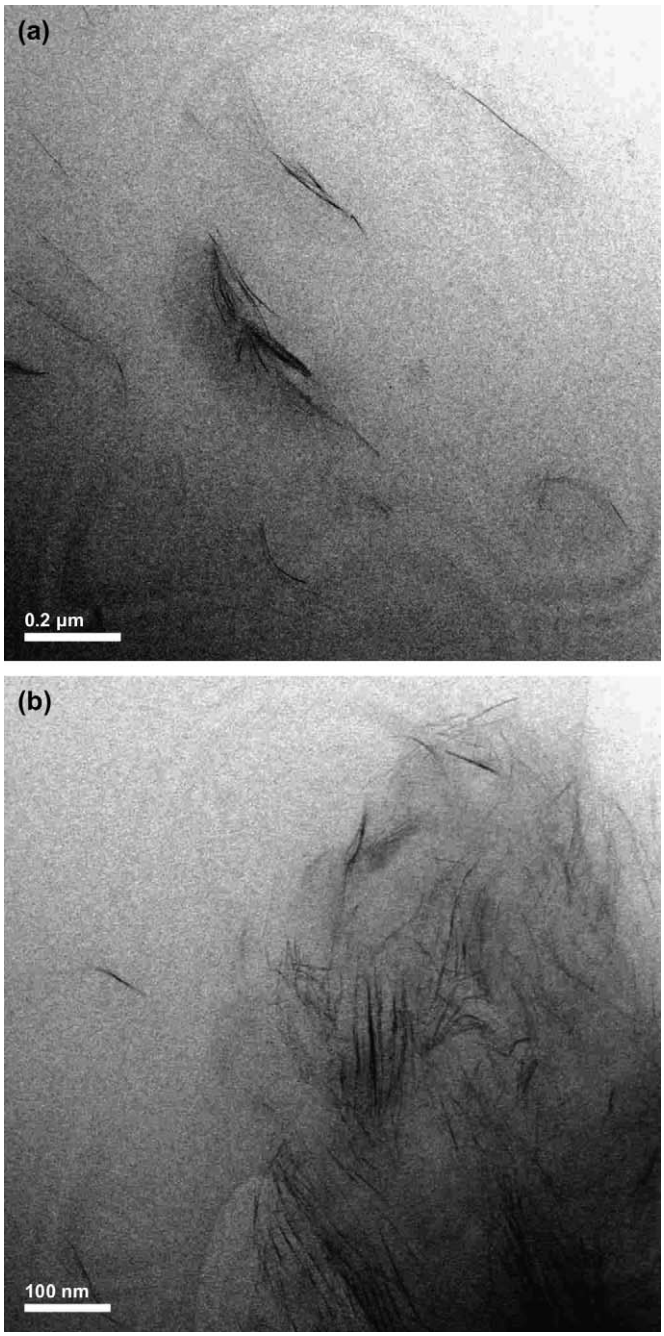

Fig. 2. TEM photomicrographs of 5 wt% clay reinforced maleated PP: (a) low magnification and (b) high magnification. Clay aggregates with intercalated structures can be observed.

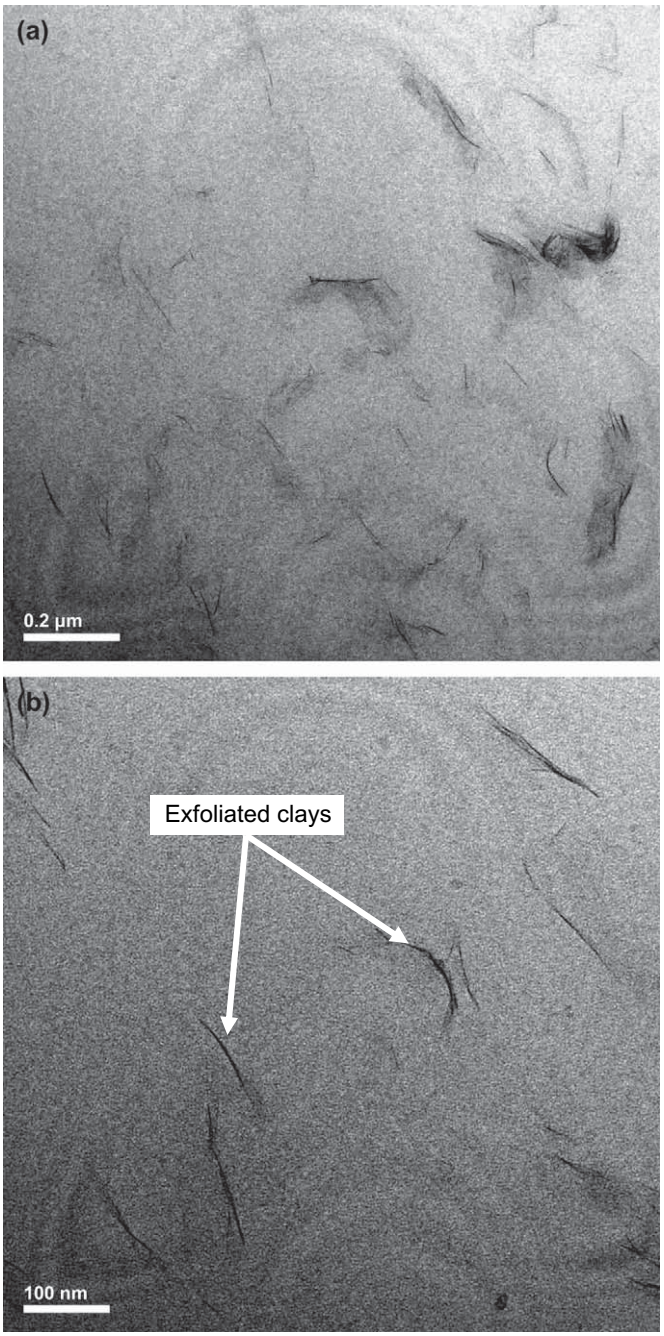

Fig. 3. TEM photomicrographs of 7.5 wt% clay reinforced maleated PP: (a) low magnification and (b) high magnification. More well exfoliated clay structures emerge.

reported independently from a different laboratory [13]. As the clays become increasingly exfoliated in extruded pellets, the driving force to separate the clay platelets are aided by increasing viscosity and shear forces, in addition to the surface chemistry and thermodynamic parameters. At the same time, the polymer chains become more confined due to the presence of exfoliated clay platelets. As a result, the fracture toughness decreases under the given loading rate whereby the polymer chains cannot deform in a timely manner before catastrophic fracture takes place.

It would be interesting to investigate the relative change in local stiffness in light of the presented micrographs. Instrumented indentation was performed on the (1) clay–polymer intercalated region, (2) the boundary region between clay aggregate and matrix, and (3) MAPP matrix alone. The positions of indentations were determined with the aid of a 40× objective lens. Indenter to microscope calibration was performed as prescribed by the manufacturer's manual. Fig. 5 shows the representative load vs. displacement curves for MAPP matrix and one for the 10 wt% clay congregated region on MAPP. The quasi-static loading curve consists of both elastic and plastic

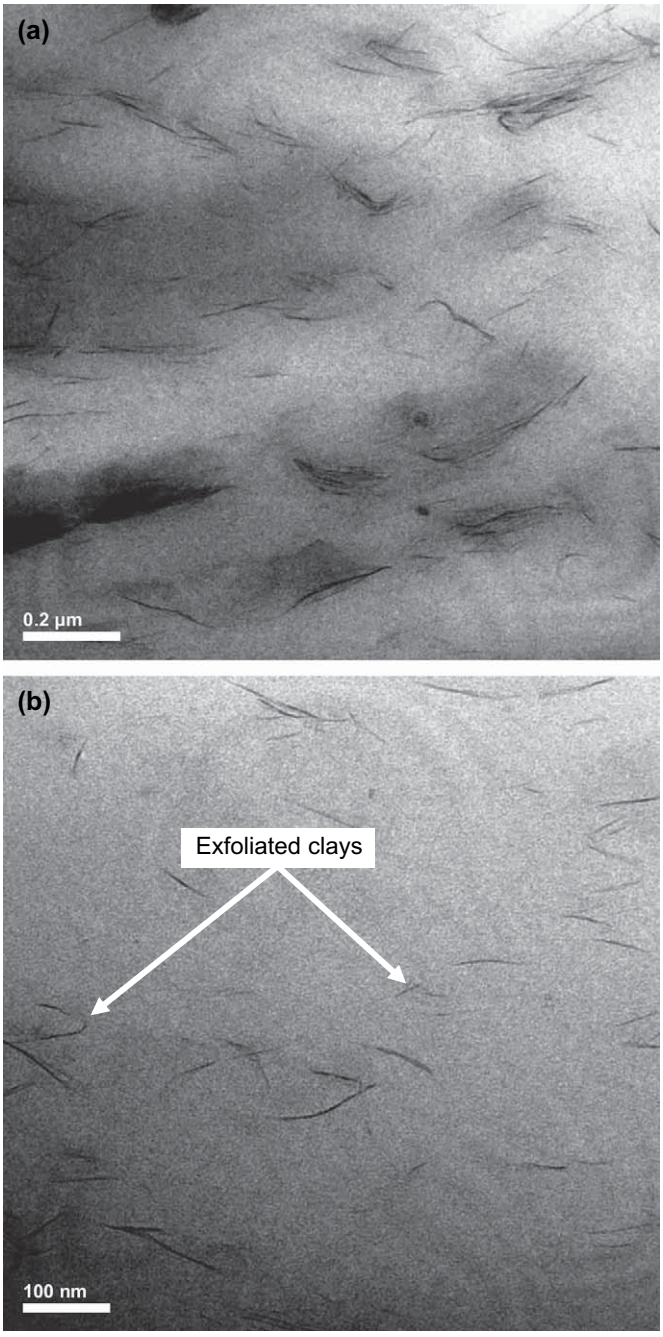

Fig. 4. TEM photomicrographs of 10 wt% clay reinforced maleated PP: (a) low magnification and (b) high magnification. Note the more uniform dispersion of clay platelets and well exfoliated clays in comparison to Figs. 1–3.

deformations. It is from the beginning of the unloading slope that the conventional elastic indentation stiffness is calculated [16]. Fig. 6 illustrates the positions where indentations were performed according to the 40× objective lens with the nanoindenter. The indentation was monitored and applied on the intercalated clay platelets, which are embedded in MAPP matrix. This region can be considered as a sub-composite system. Image analysis of a range of TEM micrographs indicates that the increase in filler content ranges from 16 to 50% by area, which is assumed to correspond to the local filler volume fraction, in the clay congregated region, but the overall weight

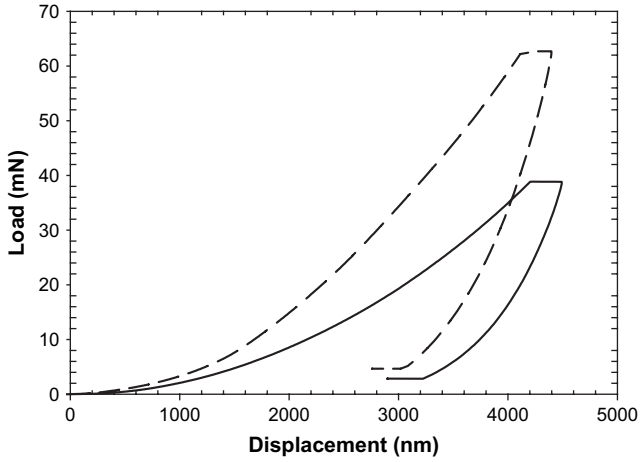

Fig. 5. Representative load vs. displacement curves for the instrumented indentation tests. The solid line (—) represents indentation on unreinforced maleated PP and the dashed line (------) represents the indentation on the clay congregated region.

fraction of clay increases with the values (0, 2.5, 5, 7.5 and 10 wt%) reported for the bulk. Fig. 7 plots the indentation stiffness as a function of indentation depth. The instrumented indenter operating under continuous stiffness measurement (CSM) can sensitively assess local stiffness as the indenter tip traverses the polished surface and the composite medium.

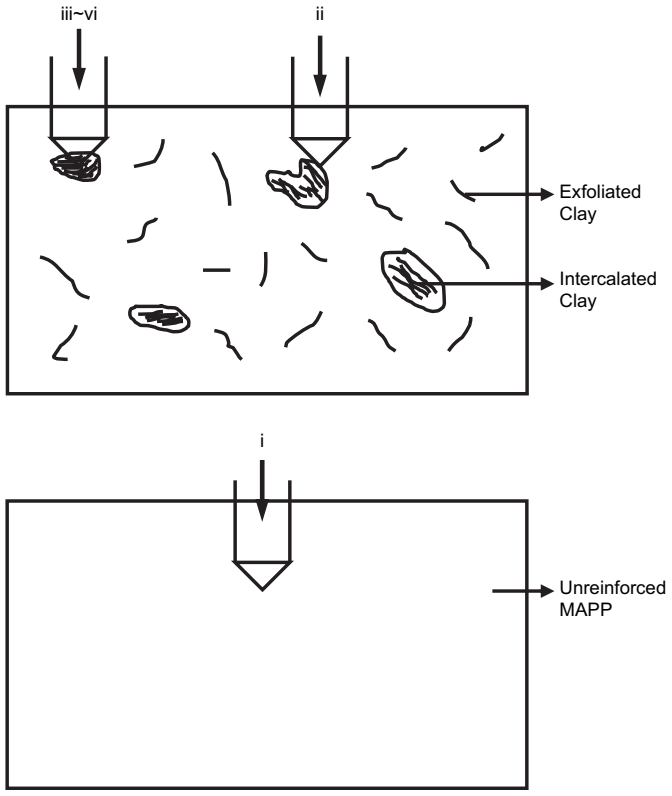

Fig. 6. Schematic indicating the observed morphology and where the nanoindentations were performed: (i) unreinforced region; (ii) clay–matrix boundary; (iii) 2.5 wt% clay congregated region; (iv) 5 wt% clay congregated region; (v) 7.5 wt% clay congregated region and (vi) 10 wt% clay congregated region.

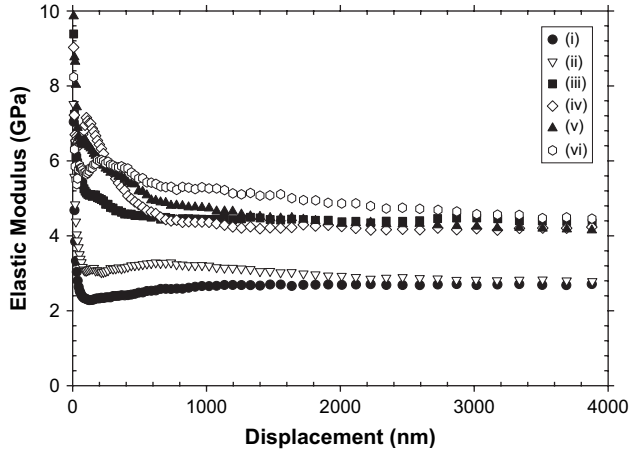

Fig. 7. Elastic modulus vs. displacement curves for (i) unreinforced region; (ii) clay–matrix boundary; (iii) 2.5 wt% clay congregated region; (iv) 5 wt% clay congregated region; (v) 7.5 wt% clay congregated region and (vi) 10 wt% clay congregated region.

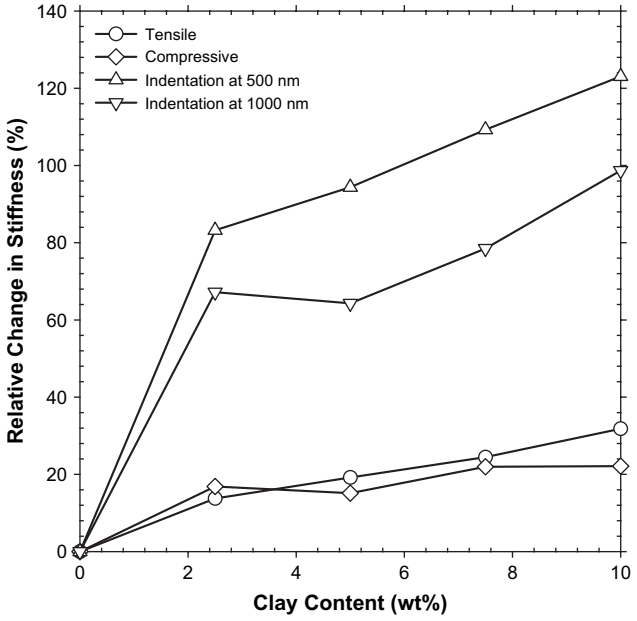

Fig. 8. Relative increase in local and global stiffnesses vs. clay content.

As anticipated, the local stiffness of the clay-containing region is much higher than that of unreinforced MAPP matrix. The clay congregated regions (2.5, 5, 7.5 and 10 wt% loadings) exhibit drastically higher local elastic stiffness as compared to the indented stiffness on MAPP matrix, up to 4000 nm. Note that at the indentation displacement less than 100 nm, the resistance against elastic deformation is generally high, consistent with other published results [17]. This is due to the indentation size effect which is physically modeled by Gao [18], that is, the smaller the indentation, the larger the Young's modulus when the indentation radius is very small. The contact area between the indenter tip and the sample surface increases as indentation displacement increases (Eq. (1)). The indenter contact area is calculated semi-empirically [16] in this study using the Nanoindenter XP software and is shown to be 7.32 μm^2 and 26 μm^2 for 500 nm and 1000 nm in displacements, respectively. Such a large contact area suffices to justify the data obtained from indenting on a comparatively homogenous structure of clay-intercalated polymer region in the nanometer scale.

Fig. 7 shows that the elastic modulus decreases and levels off steadily as the indentation depth increases. Some anomalies can be seen in the region of a few hundred nm in displacement for the clay congregated regions. The anomalies are understood when the indenter interacts with the various geometries of clay galleries and stacking orders such as those observed in Fig. 1b. Fig. 7 by no means indicates that the clay congregated regions will continue to give rise to higher local stiffness as the indenter traverses beyond the clay (>4000 nm), which is embedded in the MAPP matrix. We conjecture that the curves representing the clay congregated regions (iii–vi) will eventually merge with those from the less congregated and unreinforced regions (i–ii) as the indenter traverses beyond the clay aggregate. This is understood because the indenter has to travel and puncture through the clay-intercalated structures and come into contact directly with MAPP on its unloading path. At present, the indentation depth at 4000 nm is far from the converging point. And, the vertical displacement beyond 300 μm of the indenter tip is limited by experimental setup and the machine design capacity for nanoindentation tests. As a result, such an assumption awaits future verification when nanoscale instrumented indentation technology advances.

At low indentation depth on clay congregated region, the relative increase in local modulus is more drastic than the relative increase in the moduli of the bulk. Fig. 8 shows the relative increase in stiffness of nanoclay-filled polypropylene modified with maleic anhydride (MA). By comparing the relative increase in stiffnesses instead of the actual stiffness, the influence of the viscoelastic effect is minimized and it is beyond the scope of our present discussion. It was reported that loading rates had little influence on the unloading stiffness of viscoelastic polymers [19]. In Fig. 8, the indentation stiffness is compared to the stiffnesses obtained from (1) standard tensile and (2) compressive tests using the specimens discussed in Section 2.1. Fig. 8 shows the relative change in stiffness, which is given by the following:

$$\Delta E_{\mathrm{L}} = \frac{E_{\mathrm{Li}} - E_{\mathrm{LPP}}}{E_{\mathrm{LPP}}} \tag{2a}$$

and

$$\Delta E_{\mathrm{G}} = \frac{E_{\mathrm{Gi}} - E_{\mathrm{GPP}}}{E_{\mathrm{GPP}}} \tag{2b}$$

where, ΔE_{L} indicates the relative increase in local stiffness and ΔE_{G} the relative increase in global stiffness. The subscripts i, L and G denote reinforced, local and global stiffnesses, respectively, and E_{LPP} and E_{GPP} are, respectively, local stiffness of unreinforced maleated PP from the nanoindenter and global stiffness of unreinforced maleated PP from the uniaxial tensile

and compressive tests. The relative change in stiffness for unreinforced PP matrix is naturally assumed to be 0 for illustrative purposes.

As the indentation depth increases on the clay congregated region, the difference between "the relative local modulus increase" and "the relative increase in modulus of the bulk" increases as a result of nanoclay reinforcement. It is understood that in the clay congregated region, the sub-composite possesses a high filler volume fraction than what is assessed from the bulk. However, the increase in local stiffness exceeds what is anticipated from the increase in local filler content which is less than 50 vol%. The results suggest that the nanoreinforcements appear to create a more potent stiffening effect on the local scale when compared to the stiffening effect predicted from composite theory. The potent stiffening effect is conjectured to be related to the molecular chain confinement and topological constraint [20] imposed by clay platelets.

As shown in Fig. 8, it is clear that stiffness increases as clay content increases and the relative change is more pronounced for lower indentation depth at 500 nm when compared to higher indentation depth at 1000 nm. The results suggest that the clay congregated regions provide considerably higher resistance against local deformation in comparison to resistance against global deformation under both tension and compression. This finding can be rationalized by the fact that the clay possesses inherent stiffness higher than the matrix and the indenter is indeed indenting on the clay in a comparatively shallow depth profile. From the clay morphology as we observed from Figs. 1–4, however, the clays are indeed intercalated in the clay congregated area, and a mixture of intercalated and exfoliated morphology can be seen. As a result, the elastic stiffness is not entirely attributable to the clay, which is intercalated and supported by the polymer matrix in the intergallery spacings and underneath the clay platelets. The local polymer confinement, and thereby reinforcement, is more significant on lower indentation depth (500 nm) as compared to one for higher indentation displacement (1000 nm). The increase in local stiffness cannot be sufficiently accounted for by the increase in local filler volume. Factors such as polymer chain confinement and topological constraint at the nanometer scale need to be considered. Future work is under way to evaluate these two important contributions to local stiffness in nanocomposites.

To qualitatively assess the role of stress state on the results presented, we also subjected precisely the same specimens studied under nanoindentation and tensile tests for macroscopic uniaxial compression. In compressive stress, the relative increase in global elastic modulus due to clay loading is interestingly similar to the tensile stiffness and the local indentation regime, which is under biaxial tension. Nevertheless, the difference between local and bulk properties is still evident, particularly at small load-point displacement (500 nm). The role of clay on local material's properties is clearly distinguishable from the lower sub-surface and more so from the bulk sample. From nanoindentation results, it was found that nanoclays play a drastically different role on the local composite properties vs. the composite bulk as a whole. Yet, some

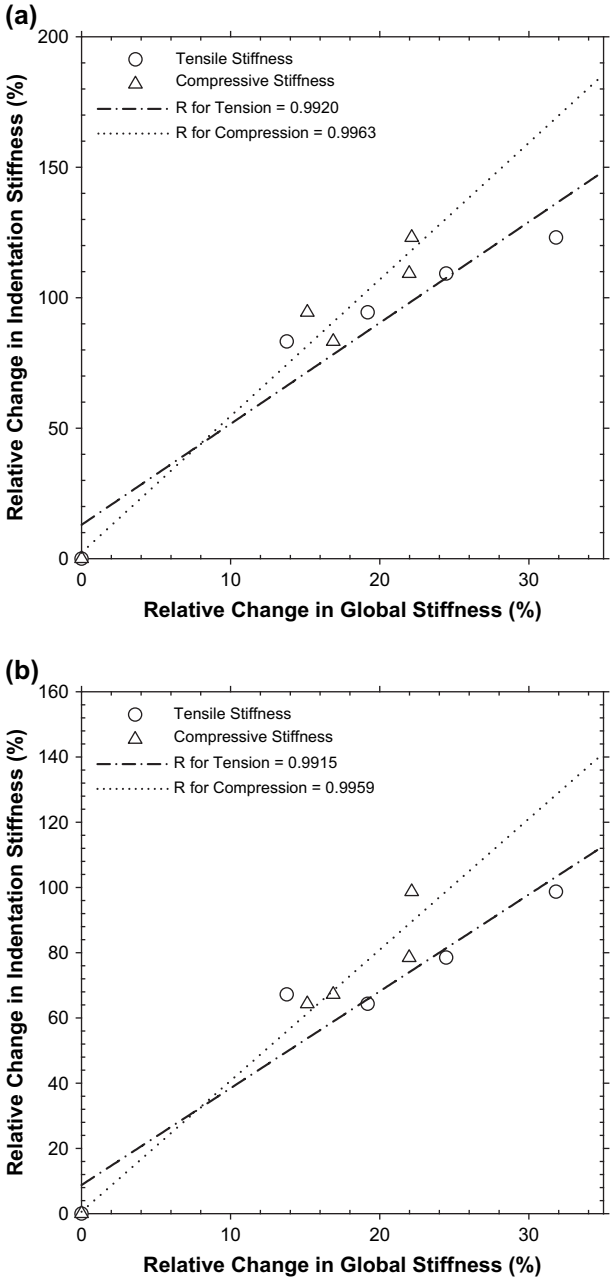

Fig. 9. Linear correlation between the % change in nanoindented stiffness and in tensile and compressive stiffnesses: (a) indentation depth = 500 nm and (b) indentation depth = 1000 nm.

degree of comparison could be observed. Fig. 9 plots the % change in indentation stiffness vs. the % change in macroscopic stiffnesses. It is clear that a rather good correlation (linear correlation coefficient, $R \sim 0.99$) could be obtained. An estimate with the least squares fit for the data in Fig. 9a shows that $\Delta E_{\text{indentation}} \sim 3.9\,\Delta E_{\text{tension}} + 13$, where $\Delta E_{\text{indentation}}$ is the % change in unloading stiffness during indentation at 500 nm and $\Delta E_{\text{tension}}$ is the % change in tensile stiffness. Likewise, $\Delta E_{\text{indentation}} \sim 5.2\,\Delta E_{\text{compression}} + 2$, where $\Delta E_{\text{compression}}$ is the % change in compressive stiffness. The value of such an estimate awaits more extensive data validation in future. Nevertheless, our results suggested that some form of scaling

law is plausible for prediction of the mechanical properties of the bulk using localized nanoindentation data.

4. Conclusions

Maleic anhydride modified polypropylene was reinforced with organomodified clays. The clay dispersion morphology showed a mixture of highly intercalated and well exfoliated structures. Exfoliation improved as clay loading increased up to 10 wt%. The enhancement in clay exfoliation was attributed to higher viscosity and mechanical shear stress as clay loading increased, which assisted the chemical driving force to peel the clay inter-gallery spacings apart. Instrumented indentation was performed on the polished samples. Indentations were chosen on (1) the clay aggregated region; (2) the clay–matrix boundary; and (3) the unreinforced MAPP matrix. The indentation stiffness for the clay congregated region was found to be twice as high as the unreinforced polymer. Such a potent stiffening effect at the local scale was attributed to the increase in local filler content as evident from image analysis. But the entire stiffening effect could not be accounted for by an increase in local filler volume fraction alone. Local polymer chain confinement and topological constraint imposed by nanoscale clay platelets are likely to contribute to the additional increase in stiffness. The difference between the stiffnesses obtained from the two distinct areas (clay congregated region and unfilled matrix) subsided as the indenter tip travels greater into the sample depth. The change in local stiffness on the clay congregated region was generally higher but remained relatively constant as the clay content increased further. Good correlation between the change in local stiffness and the change in global stiffness was obtained ($R \sim 0.99$). The results suggested that some form of a scaling law is potentially plausible to predict mechanical properties of the bulk using highly local indentation methods.

Acknowledgements

SCW thanks the National Science Foundation for the support of this research under Award# DMI-0520967. SM also thanks the Air Force Office of Scientific Research (Dr. Les Lee) for support of the research project.

References

[1] Chen L, Wong SC, Sreekumar P. J Appl Polym Sci 2003;88(14):3298–305.
[2] Kojima Y, Usuki A, Kawasumi M, Okada A, Fukushima Y, Kurauchi T, et al. J Mater Res 1993;8(5):1185–9.
[3] Cho JW, Paul DR. Polymer 2001;42(3):1083–94.
[4] Chen L, Wong SC, Liu TX, Lu XH, He CB. J Polym Sci Part B Polym Phys 2004;42(14):2759–68.
[5] Nair SV, Goettler LA, Lysek BA. Polym Eng Sci 2002;42(9):1872–82.
[6] Li Y, Wei GX, Sue HJ. J Mater Sci 2002;37(12):2447–59.
[7] Messersmith PB, Giannelis EP. J Polym Sci Part A Polym Chem 1995;33(7):1047–57.
[8] Kato M, Tsukigase A, Tanaka H, Usuki A, Inai I. J Polym Sci Part A Polym Chem 2006;44(3):1182–8.
[9] Gain O, Espuche E, Pollet E, Alexandre M, Dubois PH. J Polym Sci Part B Polym Phys 2005;43(2):205–14.
[10] Wong JSS, Sue HJ, Zeng KY, Li RKY, Mai YW. Acta Mater 2004;52(2):431–43.
[11] Odegard GM, Bandorawalla T, Herring HM, Gates TS. Characterization of viscoelastic properties of polymeric materials through nanoindentation. In: Proceedings of the 2003 SEM annual conference and exposition on experimental applied mechanics. Charlotte, NC; June 2–4, 2003.
[12] Wang K, Wang L, Wu J, Chen L, He C. Langmuir 2005;21(8):3613–8.
[13] Wang K, Chen L, Wu J, Toh ML, He C, Yee AF. Macromolecules 2005;38(3):788–800.
[14] Chen L, Wang K, Toh ML, He C. Macromol Mater Eng 2005;290: 1029–36.
[15] Lee HS, Fasulo PD, Rodgers WR, Paul DR. Polymer 2005;46:11673–89.
[16] Oliver WC, Pharr GM. J Mater Res 2004;19(1):3–20.
[17] Shen L, Phang IY, Chen L, Liu T, Zeng K. Polymer 2004;45(10):3341–9.
[18] Gao XL. J Mater Res 2006;21:1317–26.
[19] Nai MH, Lim CT, Zeng KY, Tan VBC. J Metastable Nanocryst Mater 2005;23:363–6.
[20] Benedict M, Maguire JF. Phys Rev 2004;B70:174112.